NON-LINEAR DYNAMICS OF WING CONTROL SURFACE WITH FREE-PLAY

Flávio D. Marques (fmarques@sc.usp.br)
Rui M. G. de Vasconcellos (ruivasc@sc.usp.br)
Thiago P. Maccagnan (thi.maccagnan@gmail.com)
Laboratory of Aeroelasticity, Engineering School of São Carlos – University of São Paulo
Av. Trabalhador Sancarlense, 400, 13566-590, São Carlos, SP, Brazil

Abstract. *Non-linear effects can degrade the aeroelastic behavior of aeronautical structures, leading to a broad range of adverse features. The presence of nonlinearities in aeroelastic analysis can be originated from both aerodynamic and structural sources. Compressibility, separated flows, aerodynamic heating and turbulence effects are some important aspects that result in non-linear aerodynamic behavior. Focusing on structural non-linearities they can be subdivided into distributed and concentrated ones. Distributed non-linearities are spread over the entire structure and may be related to material properties and/or large deformations. Concentrated non-linearities act locally, typically associated with loose attachments, friction, and worn hinges, for instance. These non-linearities can be approximated by classical non-linearity modeling, namely, polynomial fitting, free-play and hysteresis, or by a combination of those. This work presents an aeroelastic analysis of a finite wing model with control surface hinge free-play. An unsteady aerodynamics model based on the vortex lattice method is used to couple with rigid control surface equation of motion. During simulations the wing main structure is also assumed rigid and fixed at a determined angle of attack, while the control surface reacts depending on the non-linear stiffness and damping parameters at its hinge. Aeroelastic evolutions are investigated to capture LCO and other non-linear phenomena. Techniques from time series theory, frequency domain analysis and the determination of Poincaré maps from reconstructed space state are also used.*

Keywords: *Non-linear aeroelasticity, LCO, bifurcation, control surface free-play.*

1. INTRODUCTION

In some aeroelastic analyses linear aerodynamics and structures are adopted and the problem is reduced to the solution of a set of linear differential equations. The results are quite accurate for a specific range of velocities and structural conditions. However, aerospace systems are inherently non-linear (Dowell *et al.*, 1978). The presence of these nonlinearities will modify the behavior of the system, neglecting some results obtained from the linear approach. For example, it is shown that the classical linear flutter behavior at a critical velocity can be converted into a periodic or chaotic motion when the non-linear analysis is assumed, i.e. the short term damages of the linear flutter are converted into long term non-linear effects (Lee and Kim, 1995).

The presence of nonlinearities in aeroelastic analysis can be divided into aerodynamic and structural properties. A nonlinear aeroelastic system can have both non-linear properties simultaneously or only one of these properties at a time. Compressibility, separated flows, aerodynamic heating and turbulence effects are important aspects that result in non-linear aerodynamic behavior; nonetheless, their modeling still is a considerable challenge and will not be treated in this paper. Lee *et al.* (1999) show a comprehensive study of the different types of aerodynamic nonlinearities present on aeroelastic systems.

In terms of structural properties the effect of aging, loose attachments, certain material features, large motions or deformations are examples of nonlinearities to be considered. Structural nonlinearities can be subdivided into distributed and concentrated ones. Distributed nonlinearities are spread over the entire structure representing the characteristic of materials and large motions, for example (Patil and Hodges, 2004; Brown, 2003). Concentrated nonlinearities act locally, representing loose of attachments, worn hinges of control surfaces, aging, and presence of external stores (Lee *et al.*, 1999; O'Neil and Strganac, 1998; Conner *et al.*, 1997). The concentrated nonlinearities can usually be approximated by one of the classical structural nonlinearities, namely, cubic, free-play and hysteresis, or by a combination of these, for example, a free-play and a cubic one.

In general a non-linear aeroelastic system has four types of responses, i.e., flutter, divergence, limit cycle oscillation (LCO) and chaotic motion (Lee and Kim, 1995). The LCO is a periodic oscillation consisting of a limited number of frequencies and amplitudes. The chaotic motion is a non-periodic oscillation consisting of a multitude of frequencies and amplitudes. In some cases the LCO and the chaotic motion can occur at a flow speed lower than the linear flutter speed, showing the importance of the non-linear assumption in aeroelastic analyses.

Many authors have examined the non-linear aeroelastic behavior. Free-play, hysteresis, and cubic stiffness nonlinearities are examined considering a 2 *dof* typical section using Wagner indicial function to represent the linear aerodynamics. It is shown that flutter velocity can be reduced by an increase in initial displacements when free-play and hysteresis cases are considered in the airfoil rotation. They also found limit cycle oscillations (LCOs) bellow the linear flutter boundary

when cubic hardening cases are considered. Free-play non-linearity for the torsion mode considering linear and non-linear aerodynamic models is also investigated by some authors (Tang and Dowell, 1993). The linear aerodynamics was modeled using the Theodorsen function, what is valid when harmonic motion is assumed. In some cases, aeroelastic analysis of a two-dimensional airfoil section with combined non-linearity of free-play and cubic stiffening in torsion are performed (Zhao and Hu, 2004).

Typical dynamical system responses can be assessed by means of reconstructing the state space from time series using the so-called method of *singular value decomposition* (SVD) (Broomhead and King, 1986). The SVD uses the properties of covariance matrix to produce uncorrelated coordinates, as result of the process, the data is filtered, avoiding complications caused by the noise, always present in experimental data. With reconstructed state spaces it is possible to identify structures associated to limit-cycle oscillations (LCO) and chaos (Nayfeh and Balachandran, 1995; Vasconcellos, 2007). Chaotic behavior may be characterized by the divergence between neighbor trajectories in state space (Hilborn, 2000). The assessment of Lyapunov exponents can be used to quantify this divergence (Nayfeh and Balachandran, 1995).

This paper presents the study of non-linear aeroelastic behavior of wing control surface with hinge free-play. The model comprises a finite wing with control surface (aileron) both considered as rigid body. The aeroelastic behavior is obtained by the control surface motion restrained by the hinge stiffness. The aeroelastic response is related to one degree of freedom problem and nonlinearity is introduced by assuming free-play ate the control surface hinge. Aerodynamic model is based on the unsteady vortex lattice method. Aeroelastic responses are obtained via numerical solution of the motion equation at each time step using a forth order Runge-Kutta method, together with Henon's approach to account for the discontinuities associated to the free-play nonlinearity. The investigation of the non-linear responses is achieved by simulating the aeroelastic system and verifying the dynamics embedded in the control surface angle, particularly for limit cycle oscillations. Frequency domain analysis is also presented revealing multiple harmonics. Finally, a Poincaré mapping is performed for a range of freestream velocities, in order to observe jumps and bifurcations.

2. AEROELASTIC MODEL

This work considers the aeroelastic responses of wing control surface alone due to unsteady aerodynamic loading. Therefore the wing main structure is admitted rigid and fixed in space at a particular angle of attack. Control surface angular reactions can be modeled as one degree of freedom problem, admitting this as rigid body.

The one *dof* control surface equation of motion is given by,

$$I\ddot{\delta}(t) + C\dot{\delta}(t) + Kf(\delta(t)) = H(t) \quad , \tag{1}$$

where I is the control surface inertia moment with respect to the hinge, C is the damping factor, K is the stiffness at the control surface hinge, $H(t)$ is the hinge moment (aerodynamic term), $\delta(t)$ is the control surface angular deflection, and $f(\delta(t))$ represents a non-linear function applied to the control surface deflection.

In Eq. (1), the last term in the left-hand side of the equation, that is, $Kf(\delta(t))$, indicates the non-linear control surface restoring moment. Here this non-linear effect is dictated by free-play, which is represented by,

$$\begin{cases} f(\delta(t)) &= \delta(t) + \delta_{fp} \quad \text{if} \quad \delta(t) < -\delta_{fp} \\ f(\delta(t)) &= \delta(t) - \delta_{fp} \quad \text{if} \quad \delta(t) > \delta_{fp} \\ f(\delta(t)) &= 0.0 \quad \text{if} \quad -\delta_{fp} < \delta(t) < \delta_{fp} \end{cases} , \tag{2}$$

where δ_{fp} is the free-play angle, thus the free-play size is $2\delta_{fp}$.

Aeroelastic solution in time domain requires numerical integration of coupled structural and aerodynamic models. Assuming that the aerodynamic loading in instant t is included to Eq. (1), the Runge-Kutta method can be used to time integration. A drawback of Runge-Kutta method, when free-play model is presented in the equation of motion, is a failure to cope with discontinuities. The origin of the problem is in the need for time derivatives computation during Runge-Kutta integration. When free-play edges are reached, great error in the derivatives occurs.

A solution for this problem has been successfully suggested and presented by Conner *et al.* (1997). They suggested the use of Henon approach (Henon, 1982) to avoid missing the correct time responses at the discontinuities. Henon's method is originally applied to explore and precisely get the Poincaré points for constructing the Poincaré mapping. The methodology is based on proceeding the conventional Runge-Kutta integration out of the free-play edges. When a free-play edge is encountered, the Runge-Kutta integration is inverted to present the states exactly at the discontinuity. Next integration point uses the recovered states at the discontinuity as condition to return to the conventional time integration.

2.1 Unsteady Vortex Lattice Method

The unsteady vortex lattice method (UVLM) consists of distributing plane vortex singularities over a lifting surface and its wake (Katz and Plotkin, 1991). The plane vortex singularities satisfy the Laplace equation and when it is combined with the uniform stream incompressible and potential flows around the wing the aerodynamic loading can be calculated.

Here, to implement the VLM, the wing has been represented by a lifting surface without thickness and discretized in quadrilateral elements (panels). A vortex ring is associated with each panel, being the leading segment of each vortex ring placed on the panel quarter chord line and its control point placed at the center of the three-quarter chord line. The wing discretization scheme is shown in Fig. 1. To guarantee that the flow streamlines pass over the lifting surface, it is necessary to satisfy the boundary condition of zero normal velocity on the wing surface. This boundary condition is applied at the control points and it results in the correct values for the vortex singularities (circulation Γ).

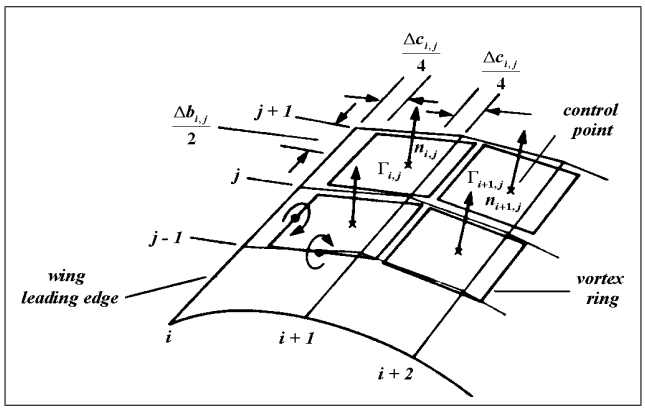

Figure 1. Wing discretization scheme (Katz and Plotkin, 1991).

The boundary condition in each panel can be expressed as

$$(\nabla\phi + v_m + v_w) \cdot \{n\} = 0 \ , \tag{3}$$

where the gradient of the potential velocity ϕ corresponds to the perturbed velocities induced by the wing vortex singularities, v_m corresponds to the velocity of the wing motion (the freestream velocity relative to the wing plus the velocities of the wing structural deformations), v_w corresponds to the velocities induced by the wake, and n is the normal vector.

The velocity V induced by each straight vortex segment, extending from point 1 to point 2, at an arbitrary point P, obeys the Biot-Savart law, that is:

$$V = \frac{\Gamma}{4\pi}\frac{r_1 \times r_2}{|r_1 \times r_2|^2}(r_1 - r_2) \cdot \left(\frac{r_1}{|r_1|} - \frac{r_2}{|r_2|}\right) \ , \tag{4}$$

where, r_1 and r_2 are the vectors that define the position of point P in relation to the points 1 and 2.

It is important to note that the value of the circulation Γ is still not known in Eq. (4). So, only the values of the other terms will be calculated. This is done by assuming $\Gamma = 1$. The velocity induced by each vortex ring at a point P is obtained adding the results obtained with Eq. (4) for the four corresponding vortex segments. The velocity is referred as the velocity induced by the vortex ring L on the control point K. Applying the zero normal velocity boundary condition at the control point $K = 1$,

$$(V_{11}\Gamma_1 + V_{12}\Gamma_2 + V_{13}\Gamma_3 + \ldots + V_{1m}\Gamma_m + v_{m1} + v_{w1}) \cdot n_1 = 0 \ , \tag{5}$$

where the circulations in each vortex ring are the unknowns and m is the number of panels used in the wing aerodynamic discretization.

Based on Eq. (5), the so-called influence coefficients ($a_{KL} = V_{KL} \cdot n_k$) can be defined. Re-writing this equation as a function of the influence coefficients for each of the m control points and passing v_m and v_w to the right-hand side (RHS) of the equation, the following linear system is obtained:

$$\begin{bmatrix} a_{11} & a_{12} & \cdots & a_{1m} \\ a_{21} & a_{22} & \cdots & a_{2m} \\ \vdots & \vdots & \ddots & \vdots \\ a_{m1} & a_{m2} & \cdots & a_{mm} \end{bmatrix} \begin{Bmatrix} \Gamma_1 \\ \Gamma_2 \\ \vdots \\ \Gamma_m \end{Bmatrix} = - \begin{Bmatrix} v_{m1} + v_{w1} \\ v_{m2} + v_{w2} \\ \vdots \\ v_{mm} + v_{wm} \end{Bmatrix} \cdot \begin{Bmatrix} n_1 \\ n_2 \\ \vdots \\ n_m \end{Bmatrix} \ . \tag{6}$$

The evaluation of v_m consists of two steps: 1) the freestream velocity is obtained moving the wing in the aft direction, and 2) the velocities of the structural deformations are obtained solving the equation of motion (*cf.* Eq. (1)). The velocities induced by the wake (v_w vector) are obtained employing the Biot-Savart law (Eq. (4)). It is important to consider that a portion of the wake is generated at each time interval, according to Fig. 2. The circulation values of the last vortex rings generated are the same as those of the trailing edge vortex rings, to satisfy the three-dimensional Kutta condition. Thus,

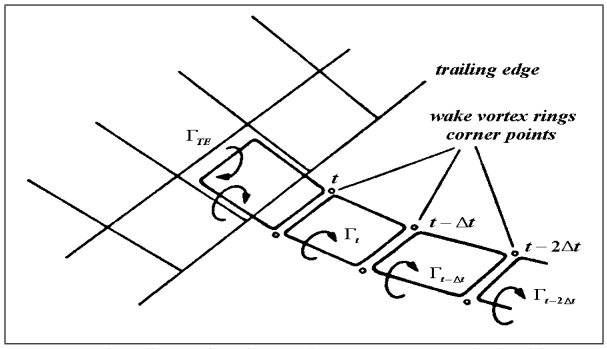

Figure 2. Wake discretization scheme (Katz and Plotkin, 1991).

at each time interval new vortex rings are generated and the corresponding values of circulation are found. The value of circulation of each wake vortex ring remains the same during all the simulation time. In the present simulation, the wake rollup has not been considered, so the wake is parallel to the freestream velocity plane.

The solution of the linear system given by Eq. (6) provides the circulation values for the wing vortex rings, which has been employed for the aerodynamic loads calculation. The unsteady Bernoulli equation for each panel is:

$$\frac{p_l - p_u}{\rho} = \frac{V_u^2}{2} - \frac{V_l^2}{2} + \frac{\partial \phi_u}{\partial t} - \frac{\partial \phi_l}{\partial t} \quad , \tag{7}$$

where p is the static pressure and the subscripts u and l refer to the upper and lower sides of the panel.

The last two terms in Eq. (7) refer to the unsteady case. The difference between them is obtained from the definition of circulation, that is:

$$\frac{\partial \phi_u}{\partial t} - \frac{\partial \phi_l}{\partial t} = \frac{\partial(\phi_u - \phi_l)}{\partial t} = \frac{\partial \Gamma}{\partial t} = \frac{\Gamma(t) - \Gamma(t-1)}{\Delta t} \quad . \tag{8}$$

If $\partial\Gamma/\partial t = 0$, Eq. (7) is analogous to the classical Bernoulli equation for the steady case, and the first two terms can be determined with the aid of the Kutta-Joukowski theorem, that is:

$$\frac{V_u^2}{2} - \frac{V_l^2}{2} = \frac{V_\infty \Gamma \Delta b cos\alpha}{S} \quad , \tag{9}$$

where V_∞ is the free stream velocity, α is the local angle of attack, Δb is the length of the panel in the spanwise direction and S is the panel area.

Substituting Eqs. (8) and (9) into Eq. (7), the pressure difference Δp_j for the jth panel can be determined, which leads directly to the aerodynamic loading terms (normal or lift forces and moments with respect to a reference point) (Katz and Plotkin, 1991).

2.2 Dynamic analysis techniques: the Poincaré mapping

A powerful tool for the verification of complex dynamics, in particular, to identify chaotic patterns is Poincaré mapping. The Poincaré section of the state space dynamics simplifies the geometric description of the dynamics by removing one of the state space dimensions. For instance, a three-dimensional state space presents the Poincaré section as a two-dimensional plane chosen in such way that the trajectories intersect it transversely.

The key point is that this simplified geometry contains the essential information about the periodicity, quasi-periodicity, chaocity and bifurcations of the system dynamics (Hilborn, 2000). Bifurcation in this case, is the term used to describe any sudden change in the dynamics of the system due to the respective parametric change. Therefore, for any change on the attractor geometry with a parameter variation, bifurcations can be visualized by plotting one Poincaré section for each parameter value. The Poincaré section computation has been based on Merkwirth *et al.* (1998) and Kantz and Schreiber (2004), which proposes the section extracted directly from an embedded time series. The result is a set of (*n-1*)-dimensional vector points, used to perform an orthogonal projection.

3. CONTROL SURFACE NON-LINEAR AEROELASTIC ANALYSIS

Aeroelastic simulations are performed for geometric and aerodynamic parameters as presented in Tab. 1. Those parameters have been based on data from literature and other values encountered in the work of Eller (2006) (based on ASK 21 glider). The aerodynamic model has been discretized using 15 panels spanwise and 20 panels chordwise, assuming rectangular wing geometry. For the control surface, the discretization corresponds to 5 chordwise per 5 spanwise panels, located at the wing tip trailing edge. The hinge line is assumed at the edges of the panels.

Table 1. Parameters for aeroelastic simulations

Description	Value
Wing chord	$1.058m$
Wing semi-span	$8.5m$
Wing angle of attack	$0°$
Control surface inertia moment (I)	$0.0336\frac{kg}{m^2}$
Damping factor (C)	$2.8Ns$
Hinge stiffness (K)	$17\frac{Nm}{rad}$
Control surface initial angle (δ_0)	$0.1°$
Freeplay angle (δ_{fp})	$0.3°$
Time sampling	$0.005s$

To check the aerodynamic solution for the unsteady problem alone, simulations have been performed for some typical control surface motions. The Fig. 3 presents two illustrations of unsteady aerodynamic solution for fixed control surface sudden wing forward acceleration (*cf.* Fig. 3(a)) and for oscillating control surface (*cf.* Fig. 3(b)). The wake arrangement due to the unsteady motion of the wing clearly shows the efficiency of the UVLM to cope with respective aerodynamic features.

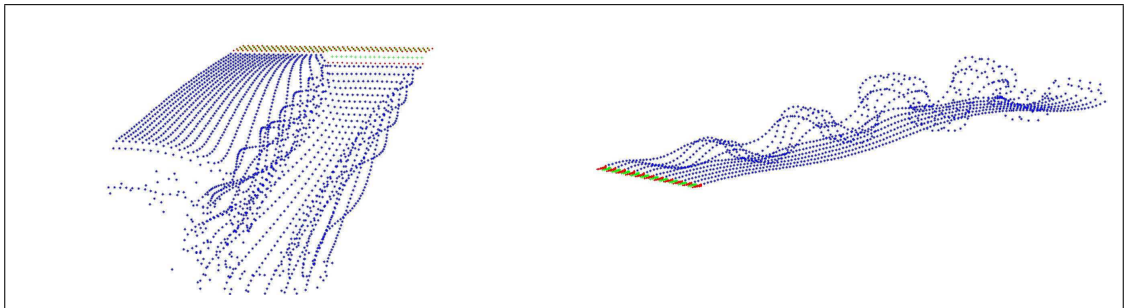

(a) Fixed control (b) Oscillating control

Figure 3. Control surface wake evolution in time for prescribed motion.

Aeroelastic simulations have been performed for a range of airspeeds from 5.0 to 45.0$\frac{m}{s}$. Particularly, for this range all simulations have revealed limit cycles oscillatory motions. Figure 4 present the time histories of $\delta(t)$ for some of the freestream velocities, depicting the typical LCO. As airflow velocity varies, it is clear from Fig. 4 the evolution on aeroelastic response amplitude and frequency composition of each resulting LCO.

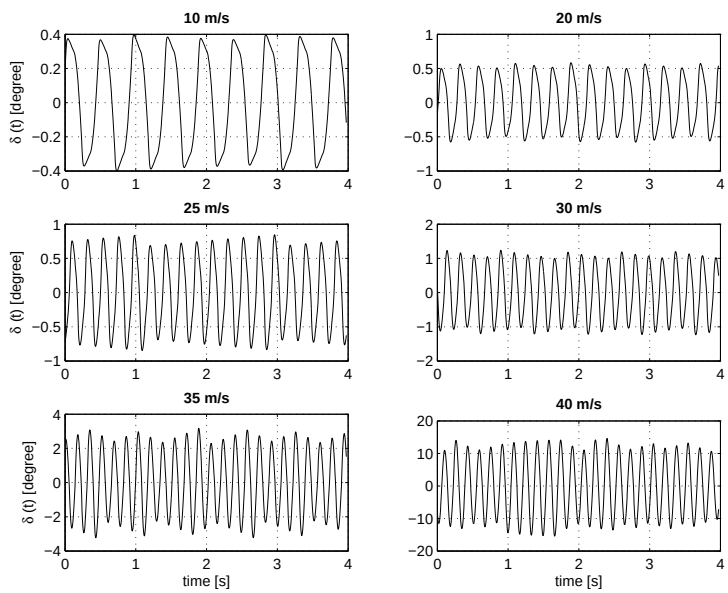

Figure 4. Control surface time responses for varying airspeed.

Other form of inspecting the LCO behavior is by plotting the phase plane $(\delta \times \frac{d\delta}{dt})_t$ for each aeroelastic signal attained during simulations at different airspeeds. These results are presented in the Fig. 5, which also can be used to identify complex features as the system evolves with the freestream velocity. These facts may also indicate that bifurcations and other complex non-linear behavior are present during aeroelastic evolution.

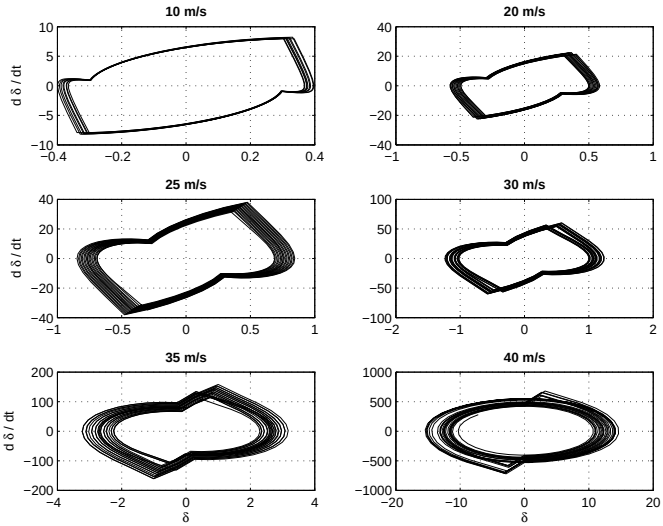

Figure 5. Phase plane of control surface response for varying airspeed.

In Fig. 6, the LCO amplitude values per airflow velocity is shown, which indicates a dramatic increase on their values after $35.0\frac{m}{s}$. Such outcome allows to infer that bifurcation phenomenon has occurred. However, the values for control surface angles at 40.0 and $45.0\frac{m}{s}$ are large enough to start compromising the aerodynamic results. Although for the non-linear analysis those values may be reasonable representations of possible physical features that are not validated in this preliminary work on control surface free-play.

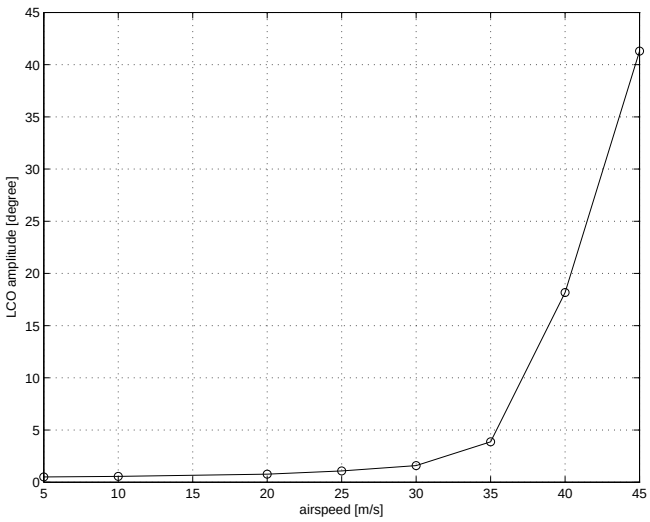

Figure 6. LCO amplitude (rms) evolution with increasing airspeed.

A frequency decomposition to the aeroelastic signals has been also executed with results presented in Fig. 7. Here the frequency content of each case clearly show the typical multiple harmonics behavior of LCO signal. The results also reinforce the conjecture that bifurcation is presented to the aeroelastic behavior of the control surface responses by inspect the sudden change in frequency content at around $30.0\frac{m}{s}$. Typically, the evolution from that airspeed would show higher multiple harmonic composition. The authors infer the this features has been not observed due to need for longer simulations that has been achieved so far by this working group.

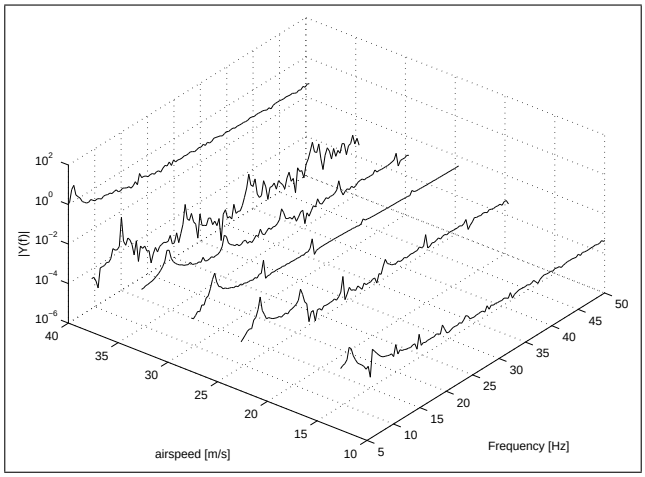

Figure 7. Control surface dynamics evolution with respect to airspeed in frequency domain.

Finally, Poincaré maps have been prepared for each freestream velocity. All mappings are presented in Fig. 8, which also reveals changes in the system behavior from around $30.0\frac{m}{s}$. One may conclude that bifurcation really happens at that condition, now reinforced by the Poincaré mapping analysis. Figure 9 complements the Poincaré analysis by showing details for four different airflow velocities. Here detailed maps also help the observe particular structures not easily highlighted in Fig. 8.

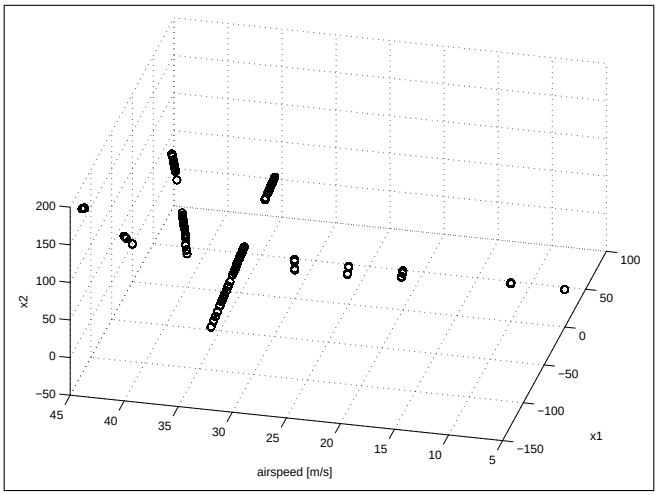

Figure 8. Poincaré mapping evolution with increasing airspeed.

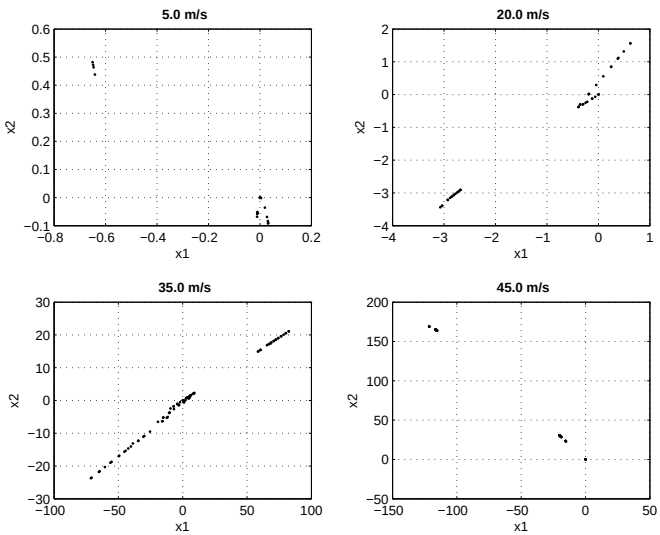

Figure 9. Poincaré mapping at particular airspeed.

4. CONCLUDING REMARKS

This work has presented an aeroelastic analysis of a finite wing model with control surface hinge free-play. The aeroelastic model is attained by coupling an unsteady aerodynamics model based on the vortex lattice method with one *dof* control surface equation of motion. During simulations the wing main structure is also assumed rigid and fixed at an angle of attack, while the control surface reacts depending on the non-linear stiffness and damping parameters at its hinge due to free-play. Aeroelastic evolutions have been investigated to capture LCO and other non-linear phenomena. Aeroelastic simulations for a range o freestream velocities have shown limit cycle oscillations of increasing amplitude as the airflow velocities increase. The frequency domain analysis has revealed multiple harmonics associated to the control surface signals, which is characteristics of LCO responses. Poincaré mappings have been also assessed, which has allowed to verify a jump phenomena at $35\frac{m}{s}$. Future developments consider complete geometric and flow parameters sensitivity analysis. Moreover, improvements to the aerodynamic model is necessary to allow better meshing. Flexible wing model is also further effort is this research.

5. ACKNOWLEDGMENTS

The authors are thankful to FAPESP, CNPq, and FAPEMIG for funding this present research work through the INCT-EIE.

6. REFERENCES

Broomhead, D.S. and King, G.P., 1986. "Extracting qualitative dynamics from experimental data". *Physica D*, Vol. 20, pp. 217–236.

Brown, E.L., 2003. *Integrated strain actuation in aircraft with highly flexible composite wings*. Ph.D. thesis, Massachusetts Institute of Technology.

Conner, M.D., Tang, D.M., Dowell, E.H. and Virgin, L.N., 1997. "Nonlinear behavior of a typical airfoil section with control surface freeplay: a numerical and experimental study". *Journal of Fluid and Structures*, Vol. 11, No. 1, pp. 89–109.

Dowell, E.H., Curtiss, H.C., Scalan, R.H. and Sisto, F., 1978. *A Modern Course in Aeroelasticity*. Sijthoff & Noordhoff, The Netherlands.

Eller, D., 2006. *On an efficient method for time-domain computational aeroleasticity*. Ph.D. thesis, Royal Institute of Technology, Stockholm, Sweeden. Also published as: Tech. Rep. TRITA/AVE 2006:1, AVE, Kungliga Tekniska Högskolan, Stockholm.

Henon, M., 1982. "On the numerical computation of poincaré maps". *Physica D: Nonlinear Phenomena*, Vol. 5, No. 2-3, pp. 412–414.

Hilborn, R.C., 2000. *Chaos and Nonlinear Dynamics: An Introduction for Scientists and Engineers;*. New York: Oxford U. Press, 2nd edition.

Kantz, H. and Schreiber, T., 2004. *Nonlinear Time Series Analysis*. Cambridge University Press, Cambridge:, 2nd edition.

Katz, J. and Plotkin, A., 1991. *Low-speed aerodynamics: from wing theory to panel methods*. McGraw-Hill, Inc.

Lee, B.H.K., Price, S. and Wong, Y., 1999. "Nonlinear aeroelastic analysis of airfoils: bifurcation and chaos". *Progress in Aerospace Sciences*, Vol. 35, No. 3, pp. 205–334.

Lee, I. and Kim, S.H., 1995. "Aeroelastic analysis of a flexible control surface with structural nonlinearity". *Journal of Aircraft*, Vol. 32, No. 4, pp. 868–874.

Merkwirth, C., Parlitz, U. and Lauterborn, W., 1998. "TSTOOL – a software package for nonlinear time series analysis". In J.A. Suykens and J. Vandewalle, eds., *Proceedings of the International Workshop on Advanced Black-Box Techniques for Nonlinear Modeling*. Katholieke Universiteit Leuven, Belgium.

Nayfeh, A.H. and Balachandran, B., 1995. *Applied Nonlinear Dynamics*. John Wiley & Sons, New York.

O'Neil, T. and Strganac, T.W., 1998. "Aeroelastic response of a rigid wing supported by nonlinear springs". *Journal of Aircraft*, Vol. 35, No. 4, pp. 616–622.

Patil, M.J. and Hodges, D.H., 2004. "On the importance of aerodynamic and structural geometrical nonlinearities in aeroelastic behavior of high-aspect-ratio wings". *Journal of Fluids and Structures*, Vol. 19, pp. 905–915.

Tang, D.M. and Dowell, E.H., 1993. "Experimental and theoretical study for nonlinear aeroelastic behaviour of a flexible rotor blade". *AIAA Journal*, Vol. 31, pp. 1133–1142.

Vasconcellos, R.M.G., 2007. *Reconstrução de Espaços de Estados Aeroelásticos por Decomposição em Valores Singulares*. Master's thesis, Universidade de São Paulo - EESC-USP. (in portuguese).

Zhao, Y.H. and Hu, H., 2004. "Aeroelastic analysis of a non-linear airfoil based on unsteady vortex lattice model". *Journal of Sound and Vibration*, Vol. 276, pp. 491–510. doi:DOI: 10.1016/j.jsv.2003.08.004.

7. Responsibility notice

The author(s) is (are) the only responsible for the printed material included in this paper